Manipulation of Majorana Modes in a Double Quantum Dot

Jesus D. Cifuentes[1] and Luis G. G. V. Dias da Silva[1]

[1] *Instituto de Física, Universidade de São Paulo, C.P. 66318, 05315–970 São Paulo, SP, Brazil*

(Dated: February 7, 2019)

Majorana fermions appearing at the edges of topological superconducting wires are a promising platform for fault-tolerant quantum computation. Novel proposals use Majorana modes tunneling inside quantum dots (QDs) to implement quantum architectures, because today's precise experimental control over the QD parameters offers the unique possibility of manipulating the Majorana modes inside multi-dot systems. The simplest case where Majorana manipulation is possible is in a double quantum dot (DQD). So far, no complete analysis of this basic structure has been done. This project fills this gap by realizing an exact quantum transport study of the effects of coupling a Majorana mode with a DQD. By tuning the model parameters we show that it is possible to control the localization of the Majorana signature in the DQD.

I. INTRODUCTION

In the last few decades the interest in the so called Majorana fermions has been increasing. The particle proposed by the physicist Ettore Majorana as the real field solution of the Dirac equation describes a fermion which is its own antiparticle, hence it has no charge nor mass. To the date no fundamental particle with these characteristics has been found. However, theoretical research predicts that Majorana Fermions emerge as quasi-particles at the boundary of certain topological superconductors. Kitaev [1] Recently, the new technological innovations allowed the observation of Majorana signatures in different topological materials.[2–5]

Despite the positive experimental results, their is still certain skepticism about the existence of Majorana Fermions. One of the reasons is that some properties of Majorana quasiparticles like the expected non-abelian statistics have not been measure. This property is of especial interest due to its promising applications in topological quantum computing. The braiding protocol based on Majorana's non-abelian statistics is the key to fault-tolerant quantum computation.[6,7]

A promising method to detect Majorana modes consists in attaching a quantum dot (QD) to the edges of a Majorana chain in the topological phase and executing transport measurements through the QD.[8] The Majorana mode at the end of the chain then leaks inside the QD[9] which produces a zero-bias conductance peak of half a quanta $\frac{e^2}{2h}$ through the dot. This is a Majorana signature which produces half of the expected peak by a regular fermion. Recently, experiments including hybrid Majorana-QD systems have been performed.[10] In addition, the similarity of this phenomenon with the Kondo effect,[11,12] where the zero-bias conductance peak takes $\frac{e^2}{h}$, motivated the study of combined Kondo-Majorana physics in this system.[13,14] This project revealed the existance of a region of parameters where both, Kondo and Majorana physics, coexist.

This idea has turned on new lights into the design of quantum architectures,[15,16] because today's precise experimental control over the parameters of QDs - energy levels, tunneling couplings, etc. - offers the unique possibility of manipulating the Majorana modes inside multi-dot systems. The simplest case where Majorana manipulation is possible is in a double quantum dot. So far, no complete analysis of this simple case has been done. The goal of this project is to fill this gap by realizing a full quantum transport study of the effects of coupling a Majorana mode with a double quantum dot. By tuning the QD gate voltages and the Majorana couplings we will be able to probe the mobility of the Majoranamodes through the dots.

We considered both interacting and non-interacting cases. For interacting systems we used a obtained the exact transport description . On non-interacting models we used a NRG approach. We found that in symmetric couplings In the non-interacting case, we confirmed that shifting the QD's gate voltage induces the Majorana to tunnel only to the other dot. In addition, an indirect coupling of the second dot could cause destructive interference with the Majorana signature. In the interacting case, the NRG simulations confirmed these results and showed that other interacting effects - Kondo effect and RKKY interactions[17–19] - could coexist with the Majorana signatures. On the other hand, when only one QD is coupled to the leads and the other Dot is attached to the QD, the Kondo effect is annihilated due to the destructive interference generated by extra dot.[20] Our study includes how the Majorana mode interacts with these two effects.

II. MODEL AND METHODS

We consider the setup shown in Figure 1 in which a Majorana mode at the edge of Topological Superconductor(TS) is coupled to a double quantum dot (DQD), which is attached to a single metallic lead. The Hamiltonian of this system can be partitioned in four terms: the DQD Hamiltonian H_{DQD} , the Lead Hamiltonian H_{Lead} , the DQD-lead interaction $H_{DQD-Lead}$ and the coupling between the DQD and the Majorana mode H_{M-DQDs} and

$$H = H_{DQD} + H_{Lead} + H_{DQD-Lead} + H_{M-DQD} \quad (1)$$

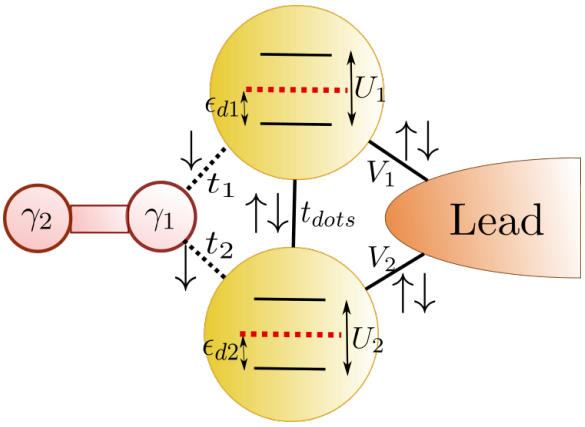

FIG. 1: DQD-Majorana set-up. Solid lines: standard coupling. Dashed lines: Majorana spin-↓ effective couplings (6). The atomic energy levels appear inside each QD. Red dashed horizontal lines represent the Fermi level.

The interacting Anderson Model describes the DQD-lead system

$$H_{DQD} = \sum_{i\in\{1,2\}}\sum_{\sigma\in\{\downarrow,\uparrow\}}\left(\epsilon_{di}+\frac{U_i}{2}\right)\hat{n}_{i\sigma}+\frac{U_i}{2}(\sum_{\sigma}\hat{n}_{i\sigma}-1)^2 + \sum_{\sigma\in\{\uparrow,\downarrow\}} t_{dots}(d^\dagger_{1\sigma}d_{2\sigma}+d^\dagger_{2\sigma}d_{1\sigma}), \tag{2}$$

and

$$H_{Lead} = \sum_{\mathbf{k}\sigma}\epsilon_{\mathbf{k}}c^\dagger_{\mathbf{k}\sigma}c_{\mathbf{k}\sigma} \tag{3}$$

$$H_{DQD-Lead} = \sum_{\mathbf{k}\sigma}\sum_{i\in\{1,2\}} V_{i\mathbf{k}}c^\dagger_{\mathbf{k}\sigma}d_{i\sigma}+V^*_{i\mathbf{k}}d^\dagger_{i\sigma}c_{\mathbf{k}\sigma}, \tag{4}$$

where ϵ_{di} is the energy level of dot i, U_i is the Coulomb repulsion and t_{dots} is the coupling parameter between both QDs. The operator $d^\dagger_{i\sigma}$ creates a particle in dot i with spin σ and $\hat{n}_{i\sigma} := d^\dagger_{i\sigma}d_{i\sigma}$ is the particle number operator of state i. $c^\dagger_{\mathbf{k}\sigma}$ is the creation operator a particle with momentum $\mathbf{k}$ and spin σ in the lead. $\epsilon_{\mathbf{k}l}$ is the corresponding energy and $V_i(\mathbf{k})$ describes the tunneling coupling between the lead and dot i .

The Majorana modes are modeled as a superposition of the creation and annihilation operators of a spin ↓ particle $f_\downarrow$

$$\gamma_1 := \frac{1}{\sqrt{2}}\left(f^\dagger_\downarrow + f_\downarrow\right), \gamma_2 := \frac{i}{\sqrt{2}}\left(f^\dagger_\downarrow - f_\downarrow\right). \tag{5}$$

This makes possible to define an effective coupling between the Majorana Mode and the DQD by attaching γ_1 with the spin-↓ channel in the QDs

$$H_{M-DQD} = \sum_{i=1}^{2} t_i\left(d^\dagger_{i\downarrow}\gamma_1+\gamma_1 d_{i\downarrow}\right)+\epsilon_M\gamma_1\gamma_2. \tag{6}$$

where t_i is the coupling parameter between the Majorana mode and QD i. ϵ_m is the coupling energy between both Majorana modes.

A. Methods

B. Non-interacting system

Using Zubarev's ballistic transport approach[21], we derived an exact expression for the Green functions associated to both quantum dot operators $(G_{d_1d_1^\dagger}(\omega), G_{d_2d_2^\dagger}(\omega))$. The detailed procedure is included in Appendix A. The transport equations define a 9×9 linear system where the Hamiltonian parameters $(t_1, t_2, \epsilon_1 \ldots)$ and the energy ω are taken as algebraic variables. The solution of this type of equations is a polynomial fraction of the same degree which makes difficult to provide an exact solution using analytical or numerical methods. To bypass this problem, we associated this transport system to a flow graph and executed a Graph-Gauss-Jordan elimination process[22]. This method proofed to be efficient to solve complex transport systems since the graph structure allows us to identify minimum cutting points and create an algorithmic representation of the Green function.

At the end, we obtained the following analytical expression

$$G_{d_{1\downarrow},d^\dagger_{1\downarrow}}(\omega) = \frac{1}{\omega-\epsilon^+_{DQD}-\frac{\|T_+\|^2}{\omega-\epsilon_{M2}-\frac{\|T_-\|^2}{\epsilon^-_{DQD}}}}. \tag{7}$$

Where

$$\epsilon^\pm_{DQD} = \pm\epsilon_1+\sum_{\mathbf{k}}\frac{V_1V_1^*}{\omega-\epsilon_{\mathbf{k}}}+\frac{\left\|\pm t_{dots}+\sum_{\mathbf{k}}\frac{V_1V_2^*}{\omega-\epsilon_{\mathbf{k}}}\right\|^2}{\omega\pm\epsilon_2-\sum_{\mathbf{k}}\frac{V_2V_2^*}{\omega-\epsilon_{\mathbf{k}}}}, \tag{8}$$

$$T_\pm = \pm t_1 \pm t_2\frac{\left(\pm t_{dots}+\sum_{\mathbf{k}}\frac{V_1V_2^*}{\omega-\epsilon_{\mathbf{k}}}\right)}{\omega\pm\epsilon_2\pm\sum_{\mathbf{k}}\frac{V_2V_2^*}{\omega-\epsilon_{\mathbf{k}}}}, \tag{9}$$

and

$$\epsilon_{M2} = \omega-\epsilon_M-\frac{\frac{\omega}{\omega+\epsilon_M}\|t_2\|^2}{\omega-\epsilon_2-\sum_{\mathbf{k}}\frac{V_2V_2^*}{\omega-\epsilon_{\mathbf{k}}}}-\frac{\frac{\omega}{\omega+\epsilon_M}\|t_2\|^2}{\omega+\epsilon_2-\sum_{\mathbf{k}}\frac{V_2V_2^*}{\omega+\epsilon_{\mathbf{k}}}}. \tag{10}$$

The final result will depend on the broadening parameter of QD i with the lead (Γ_i). This broadening satisfies the equation

$$-i\Gamma_i = \lim_{s\to 0}\sum_{\boldsymbol{k}} \frac{V_i^* V_i}{\omega + is - \epsilon_{\boldsymbol{k}}}. \tag{11}$$

By convention we take Γ_1 as the energy unit for the rest of the project. Finally we compute the DOS

$$\rho_{1\sigma}(\omega) = -\frac{1}{\pi}\mathrm{Im}\left[G_{d_{1\sigma},d_{1\sigma}^\dagger}(\omega)\right]. \tag{12}$$

Similar results can be obtain for the DOS of the second $\rho_{2\sigma}$ by exchanging the indexes 1 and 2 in equation (7).

The density of states provides significant information about the presence of a Majorana zero modes in the dot. The Majorana signature is characterized by a robust zero-mode with height equal to: 1) $\frac{0.5}{\pi\Gamma}$ or 2) The half of the spin-↑ DOS. Considering that only the spin-↓ channel is connected to the Majorana mode and that the spin-↑ and spin-↓ channels are decoupled in non-interacting systems, the existence of this second type of Majorana signature is intriguing.

C. Interacting case (NRG)

The Numerical Renormalization Group (NRG)[12,23,24] is the most successful methods to study interacting quantum impurity models. In this project, the impurity is described by the DQD attached to a Majorana mode. Our code a coulomb repulsion factor of $U = 17.3\Gamma_1$ in both dots and a cut-off energy of $D = 2U = 34.6\Gamma_1$. The spacing with other energy levels is assumed to be higher than D, such that only the two coulomb states are relevant for the system dynamics. Particle-Hole-Symmetry at each dot is obtained when $\epsilon_i = \frac{U}{2}$ in both dots. At this point, each dot has an odd number of electrons, hence, at sufficiently low temperature the system will exhibit the characteristic Kondo peaks at the Fermi energy Wilson[12]. The coexistence of Kondo and Majorana zero modes is still a point of contention in the area and one of the objectives of this part of the project

To improve the efficiency of the code we used the symmetries of the system to maintain a block structure during NRG's iterative diagonalization process. This model preserves the spin-↑ particle number $\hat{N}_\uparrow$ and the spin-↓ parity $\hat{P}_\downarrow = \pm$ (+ even, − odd). The spin-↓ particle number is not preserved due to superconducting-type Majorana coupling (6) . The initial Hamiltonian is organized in blocks according to these symmetries. This block structure is preserved during the entire iteration process[24]. To compute the spectral functions, we use the density matrix renormalization group (DM-NRG)[25] in combination with the renown Z-trick method[26], which improves spectral resolution at high energies.

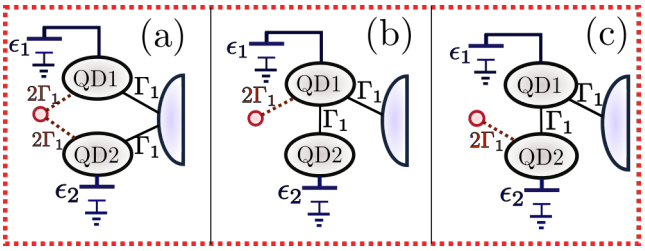

FIG. 2: Cases of study: (a) Symmetric coupling of the DQD to the lead and the MZM. No inter-dot coupling. (b)&(c) Indirect coupling of the second QD through the first dot. The Majorana is coupled to the (b) first dot or to the (c) second dot.

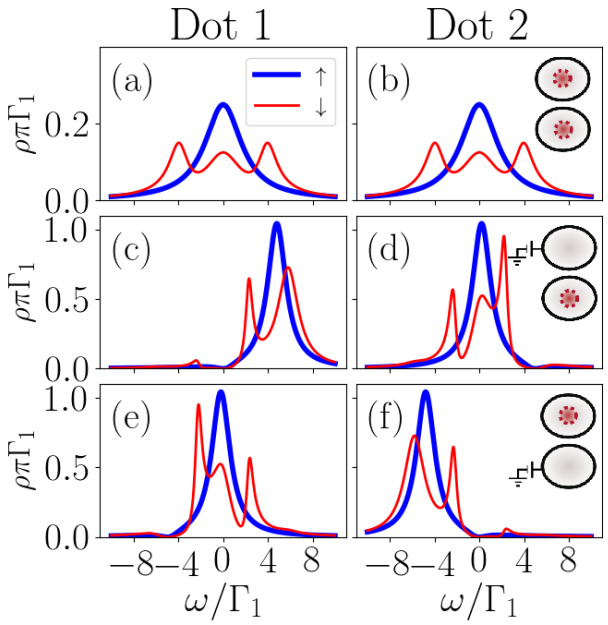

FIG. 3: Non-interaction DOS in the symmetric coupling setup (Fig.2(a)). Bold blue lines: Spin-↑ DOS. Thin red lines: Spin-↓ DOS.

III. RESULTS

A. MZM manipulation in non-interacting quantum dots

We call MZM manipulation to the "movements" attributed to the Majorana signature under the tunning of the dot gate voltages (ϵ_1, ϵ_2). This manipulation process is performed in three different set ups that are presented in Fig.2 with definite values of Γ_2, t_dots, t_1 and t_2. In configuration (a), we coupled the QD symmetrically to the lead and the Majorana mode. With this setup we expect to break the localization of the MZM which should split and tunnel into both dots. In setups (b) and (c) we coupled the second dot indirectly through the first dot.

Hence, quantum interference should split the zero mode in two states. Our objective is to observe what occurs with the Majorana signature in this case. There are to options to connect the MZM in this situation. Attached it directly through the first dot (b) or indirectly through the second dot (c).

The non-interacting results for setups (a),(b) and (c) of FIG.2 are shown at figures FIG.7, FIG.4 and FIG.5 respectively. Each figure depicts the DOS of dot 1(left) and dot 2(right). The gate voltage is initially 0 in both dots at the first row. In the second row the gate voltage is turned on to $\epsilon_1 = 5\Gamma_1$ in the first dot and remains at $\epsilon_2 = 0$ in the second dot. In the third row the first dot's voltage is off $\epsilon_1 = 0$ and we turn on the second dot with a negative voltage of $\epsilon_2 = -5\Gamma_1$. The insets at each row shows which dots exhibit Majorana signatures, depicted by a red dashed circle inside the dot. These images will continuously change under the tuning of gate voltages which represents the manipulation of the Majorana signature.

In FIG.7 we observe the results for the symmetric coupling setup FIG.2(a). In the particle hole symmetric case (first row) the DOS is equal in both dots. Note that that the spin-↓ (Thin red line) DOS is the half of the spin-↑ (Bold blue line) DOS at the Fermi energy ($\rho_\downarrow(0) = \frac{1}{2}\rho_\uparrow(0)$). This Majorana signature is similar to the one observed when a single dot is coupled to a Majorana mode.[8] We may conclude that the Majorana in tunneling inside both dots breaking the localization of the MZM. If a positive or negative gate voltage is induced in one of the dots, as shown in the second and third row of Figure 7(c)-(f), the Majorana zero mode vanishes from that dot. Meanwhile the density of states in the other dot increases while preserving the Majorana signature. This means that the MZM is actually being induced to "leave" this dots and leak into the other dot by the gate voltage activation. This first example of MZM manipulation.

Another example of MZM manipulation occurs when the second dot is not directly connected to the lead. In this case, the inter-dot tunneling generates quantum interference which finally destroys the central peak as observe in FIG.4(a) at the spin-↑ DOS . The spin-↓ channel at FIG.4(a), which is coupled to the MZM, does not exhibit the characteristic Fermi peak either. Instead, the one half Majorana signature at the Fermi energy ($\rho_\downarrow(0) = \frac{1}{2}\rho_\uparrow(0)$) appears clearly inside the second dot FIG.4(b). This situation prevails when the first dot's gate voltage is turned on FIG.4(c)&(d). While the first dot does not seem to exhibit any type of Majorana signature, the second dot's spin-↓ DOS exhibits a robust zero-mode of height $\frac{0.5}{\pi\Gamma}$. The results are more exciting when the second dot's gate voltage is turned on in FIG.4(e)&(f). These figures clearly show how the MZM, previously localized at the second dot, is induced to leave this dot and returned onto the first dot. Moreover, the DOS of spin-↑ and spin-↓ channels are very similar to the spectral densities observed at FIG.7(d)&(e) which pinpoints that the previous interference pattern has disappeared due to the presence of this gate voltage.

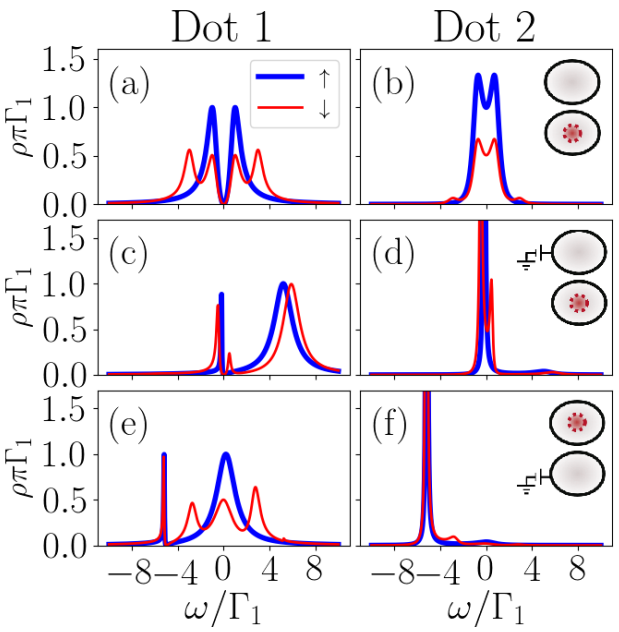

FIG. 4: Non-interaction DOS of the setup in Fig.2(b) . Bold blue lines: Spin-↑ DOS. Thin red lines: Spin-↓ DOS.

On the other hand, if the Majorana mode is attached to the second dot in the previous arrangement, then both dots will exhibit a majorana signature. However, the signature in dot 1 is different from the others. The spin-↓ DOS reveals the emergence of a zero mode with height close to 5.2 (such that $\pi\Gamma_1\rho_\downarrow(0) = 0.5$). However the spin-↑ DOS remains equal to 0. This new type of majorana signature is the result of an indirect connection between QD1 and the majorana mode attached t the second dot. As in the previous case, turning on the gate voltage in dot 1 destroys the majorana signature in both dots. However, if the gate voltage in dot 2 is turned on, the Majorana mode will leave QD2 but the indirect majorana signature will prevail in QD1.

To sum up we were able to distinguish two types of majorana signatures:

- **Type I:** The spin-↓ DOS is the half of the spin-↑ DOS at the Fermi energy ($\rho_\downarrow(0) = \rho_\uparrow(0)$).
- **Type II:** The spin-↓ Fermi energy is equal about 5.2. This is the value such that $\pi\Gamma_1\rho_\downarrow(0) = 0.5$, characteristic of a decay of half a quanta in the conductivity.

The state of these signatures for each of these stated is depicted in FIG.2. A solid filled red circle inside the dot represents the appearance of a Type I Majorana signature, on the othere hand a dashed filled red circle represents the presence a Type II Majorana signature. The obscure dashed circle represents a vanishing majorana

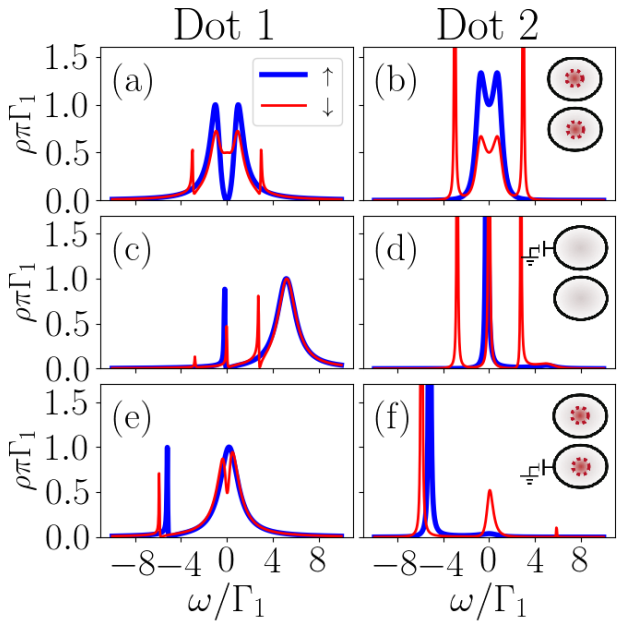

FIG. 5: Non-interaction DOS of the set up in Fig.2(c) . Bold blue lines: Spin-↑ DOS. Thin red lines: Spin-↓ DOS..

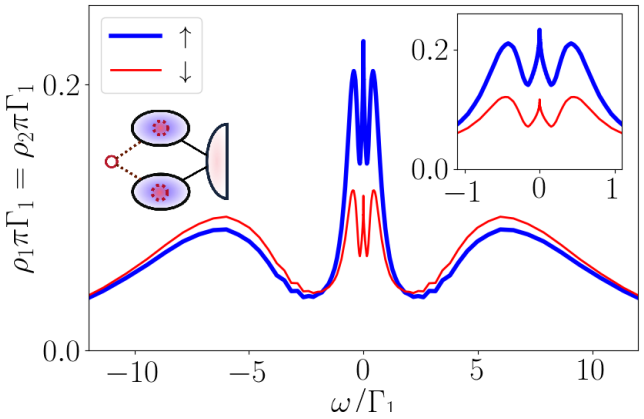

FIG. 6: Density of states of both dots in the symmetric coupling case between the Majorana and the interacting DQD. Bold blue lines: Spin-↑ DOS. Thin red lines: Spin-↓ DOS.

signature due to an applied gate voltage or by quantum interference.

B. Majorana manipulation in interacting dots

We consider a Coulomb repulsion energy of $U = 17\Gamma_1$ in both dots. The factor $\frac{U_i}{2}(\sum_\sigma \hat{n}_{i\sigma} - 1)^2$ in (2) favors states with an odd number of electrons. In addition, particle-hole equilibrium is now achieved when

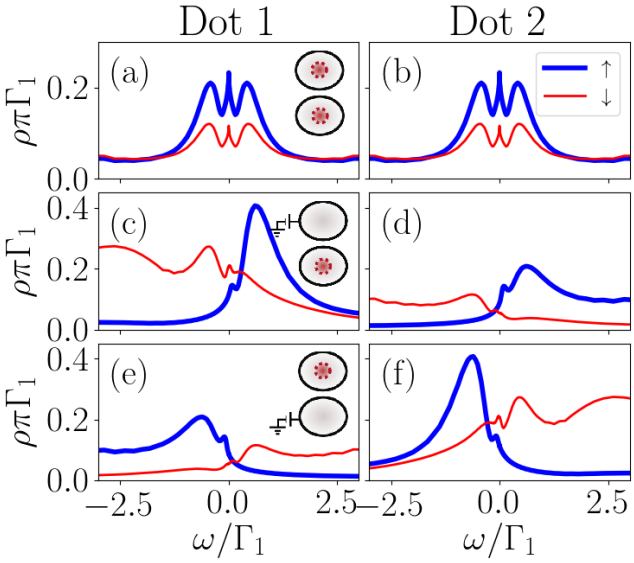

FIG. 7: Density of states in the symmetric coupling arrangement (Fig.2 first column). Bold blue lines: Spin-↑ DOS. Thin red lines: Spin-↓ DOS.

$\left(\epsilon_{di} + \frac{U_i}{2}\right)\hat{n}_{i\sigma}$. Any induced gate voltage must be considered as a shifting from this equilibrium point. In the case of symmetric coupling FIG6 shows the DOS in both QDs. The two peaks appearing at $8.6\Gamma_1 = \frac{U_i}{2}$ represent the two energy levels. The central spin-↑ peak is produced by the Kondo effect,[11,12] while the two satellite peaks observed in the inset observed are the result of the RKKY anti-ferromagnetic interaction between bott dots.[17–19] The spin-↓ DOS at the fermi energy is exactly the half of the spin-↑ DOS as expected from a Type I majorana signature. Note, that in this case the majorana signature coexists with the Kondo effect in the DQD as already predicted by Ruiz-Tijerina *et al.* for a single dot.[14]

IV. CONCLUDING REMARKS

Conclusion goes here.

ACKNOWLEDGMENTS

The authors thank Edson Vernek for enlightening discussions. L.G.G.V.D.S. acknowledges financial support by CNPq (grants No. 307107/2013-2 and 449148/2014-9), and FAPESP (grant No. 2016/18495-4).

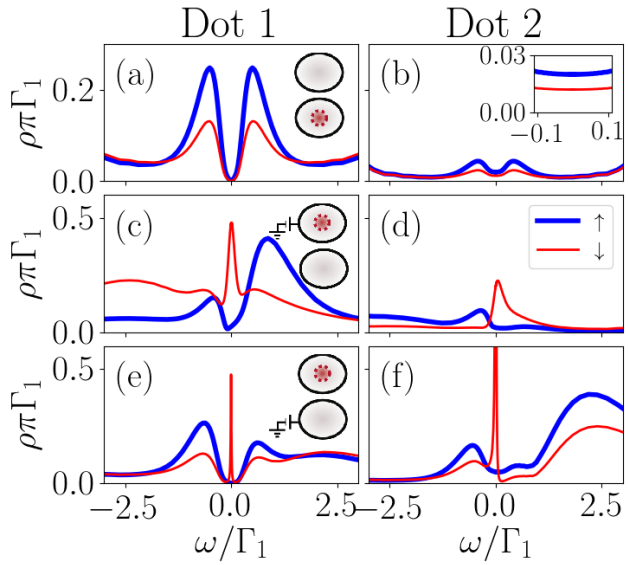

FIG. 8: Density of states in both dots of the case where the only the first QD is attached to both Majorana and Lead (Fig.2 second column) . Bold blue lines: Spin-↑ DOS. Thin red lines: Spin-↓ DOS.

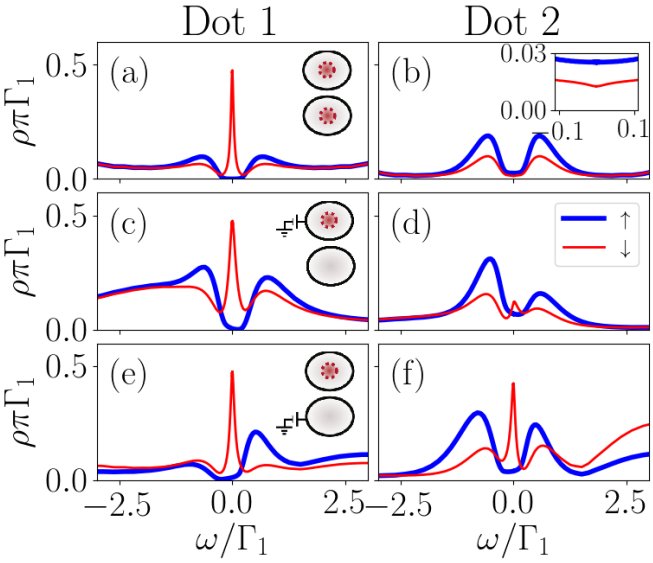

FIG. 9: Density of states of both dots in the case where only de first QD is attached to the lead and the Majorana mode is attached to the second QD. (Fig.2 third column) . Bold blue lines: Spin-↑ DOS. Thin red lines: Spin-↓ DOS.

[1] A. Y. Kitaev, Physics-Uspekhi **44**, 131 (2001).
[2] V. Mourik, K. Zuo, S. M. Frolov, S. R. Plissard, E. P. a. M. Bakkers, and L. P. Kouwenhoven, Science **336**, 1003 (2012).
[3] A. Das, Y. Ronen, Y. Most, Y. Oreg, M. Heiblum, and H. Shtrikman, Nature Physics **8**, 887 (2012).

[4] M. T. Deng, C. L. Yu, G. Y. Huang, M. Larsson, P. Caroff, and H. Q. Xu, Nano Letters **12**, 6414 (2012).
[5] H. Zhang, C.-X. Liu, S. Gazibegovic, D. Xu, J. A. Logan, G. Wang, N. van Loo, J. D. S. Bommer, M. W. A. de Moor, D. Car, R. L. M. Op het Veld, P. J. van Veldhoven, S. Koelling, M. A. Verheijen, M. Pendharkar, D. J. Pennachio, B. Shojaei, J. S. Lee, C. J. Palmstrøm, E. P. A. M. Bakkers, S. D. Sarma, and L. P. Kouwenhoven, Nature **556**, 74 (2018).
[6] A. Y. Kitaev, Annals of Physics **303**, 2 (2003), arXiv: quant-ph/9707021.
[7] S. D. Sarma, M. Freedman, and C. Nayak, npj Quantum Information **1**, 15001 (2015).
[8] D. E. Liu and H. U. Baranger, Physical Review B **84** (2011), 10.1103/PhysRevB.84.201308, arXiv: 1107.4338.
[9] E. Vernek, P. H. Penteado, A. C. Seridonio, and J. C. Egues, Physical Review B **89**, 165314 (2014).
[10] M. T. Deng, S. Vaitiekenas, E. B. Hansen, J. Danon, M. Leijnse, K. Flensberg, J. Nygard, P. Krogstrup, and C. M. Marcus, Science **354**, 1557 (2016).
[11] A. C. Hewson, *The Kondo Problem to Heavy Fermions* (Cambridge University Press, 1997) google-Books-ID: fPzgHneNFDAC.
[12] K. G. Wilson, Reviews of Modern Physics **47**, 773 (1975).
[13] M. Lee, J. S. Lim, and R. Lopez, Physical Review B **87**, 241402 (2013).
[14] D. A. Ruiz-Tijerina, E. Vernek, L. G. G. V. Dias da Silva, and J. C. Egues, Physical Review B **91**, 115435 (2015).
[15] M. Barkeshli and J. D. Sau, arXiv:1509.07135 [cond-mat, physics:quant-ph] (2015), arXiv: 1509.07135.
[16] T. Karzig, C. Knapp, R. M. Lutchyn, P. Bonderson, M. B. Hastings, C. Nayak, J. Alicea, K. Flensberg, S. Plugge, Y. Oreg, C. M. Marcus, and M. H. Freedman, Physical Review B **95**, 235305 (2017).
[17] M. A. Ruderman and C. Kittel, Physical Review **96**, 99 (1954).
[18] T. Kasuya, Progress of Theoretical Physics **16**, 45 (1956).
[19] K. Yosida, Physical Review **106**, 893 (1957).
[20] L. G. G. V. Dias da Silva, N. Sandler, K. Ingersent, and S. E. Ulloa, Physica E: Low-dimensional Systems and Nanostructures **40**, 1002 (2008).
[21] D. N. Zubarev, Soviet Physics Uspekhi **3**, 320 (1960).
[22] D. A. Spielman, *Algorithms, Graph Theory, and Linear Equations in Laplacian Matrices*, Proceedings of the International Congress of Mathematicians (2010).
[23] M. Sindel, *Numerical Renormalization Group studies of Quantum Impurity Models in the Strong Coupling Limit*, Text.PhDThesis, Ludwig-Maximilians-Universität München (2005).
[24] R. Bulla, T. A. Costi, and T. Pruschke, Reviews of Modern Physics **80**, 395 (2008).
[25] W. Hofstetter, Physical Review Letters **85**, 1508 (2000).
[26] W. C. Oliveira and L. N. Oliveira, Physical Review B **49**, 11986 (1994).

Appendix A: Computation of the Green Function

In Zubarev's fermionic ballistic transport approach[21] the green functions associated to two operators $A(t)$, $B(t)$ is defined as that Fourier transform of the time-ordered anti-commutator of A and B

$$G_{A,B}(\omega) = \mathcal{F}\left\{\mathcal{T}\left[\{A(t), B(t')\}\right]\right\}(\omega)\,. \tag{A1}$$

The Fourier transform of Schrodinger evolution determines the transport equations

$$\omega G_{A,B}(\omega) = \delta_{A^\dagger,B} + G_{[A,H],B}(\omega). \tag{A2}$$

We can apply this to Hamiltonian (1) by replacing A and B by the creation and annihilation operators. To simplify the complexity of the system we fix $B = d^\dagger_{1\downarrow}$. In addition note that the transport equations for $f_\downarrow$ and $f^\dagger_\downarrow$ are

$$(\omega - \epsilon_M)\, G_{f_\downarrow, d^\dagger_{1\downarrow}}(\omega) = \frac{t}{\sqrt{2}}\left(G_{d_{1\downarrow}, d^\dagger_{1\downarrow}}(\omega) - G_{d^\dagger_{1\downarrow}, d^\dagger_{1\downarrow}}(\omega)\right) \tag{A3}$$

$$(\omega + \epsilon_M)\, G_{f^\dagger_\downarrow, d^\dagger_{1\downarrow}}(\omega) = \frac{t}{\sqrt{2}}\left(G_{d_{1\downarrow}, d^\dagger_{1\downarrow}}(\omega) - G_{d^\dagger_{1\downarrow}, d^\dagger_{1\downarrow}}(\omega)\right), \tag{A4}$$

which allows us to take $G_{f^\dagger_\downarrow, d^\dagger_{1\downarrow}}(\omega) = \frac{\omega+\epsilon}{\omega-\epsilon} G_{f^\dagger_\downarrow, d^\dagger_{1\downarrow}}(\omega)$. Therefore, we can eliminate $G_{f^\dagger_\downarrow, d^\dagger_{1\downarrow}}(\omega)$ from the equations even before we start Gauss-Jordan process.

Writing the other equations we obtain the linear system

$$\mathcal{T}\vec{G}_{d^\dagger_1} = \hat{e_1} \tag{A5}$$

where $\mathcal{T}$ is the transport matrix

$$\begin{bmatrix}
\omega-\epsilon_1 & -V_1^* & -t_{dots} & \frac{-t_1}{\sqrt{2}} & 0 & 0 & 0 \\
-V_1 & \omega-\epsilon_k & -V_2 & 0 & 0 & 0 & 0 \\
-t^*_{dots} & -V_2^* & \omega-\epsilon_2 & \frac{-t_2}{\sqrt{2}} & 0 & 0 & 0 \\
\frac{-\sqrt{2}t_1^*}{\omega+\epsilon_M} & 0 & \frac{-\sqrt{2}t_2^*}{\omega+\epsilon_M} & \omega-\epsilon_M & \frac{\sqrt{2}t_2^*}{\omega+\epsilon_M} & 0 & \frac{\sqrt{2}t_1^*}{\omega+\epsilon_M} \\
0 & 0 & 0 & \frac{t_2}{\sqrt{2}} & \omega+\epsilon_2 & V_2^* & t^*_{dots} \\
0 & 0 & 0 & 0 & V_2 & \omega+\epsilon_k & V_1 \\
0 & 0 & 0 & \frac{t_1}{\sqrt{2}} & t_{dots} & V_1^* & \omega+\epsilon_1
\end{bmatrix}, \tag{A6}$$

$\vec{G}_{d^\dagger_1}$ is the column vector

$$[G_{d_{1\downarrow}, d^\dagger_{1\downarrow}}(\omega), G_{c_{k\downarrow}, d^\dagger_{1\downarrow}}(\omega), G_{d_{2\downarrow}, d^\dagger_{1\downarrow}}(\omega), G_{f_\downarrow, d^\dagger_{1\downarrow}}(\omega), G_{d^\dagger_{2\downarrow}, d^\dagger_{1\downarrow}}(\omega), G_{c^\dagger_{k\downarrow}, d^\dagger_{1\downarrow}}(\omega), G_{d^\dagger_{1\downarrow}, d^\dagger_{1\downarrow}}(\omega)]^T$$

and $\hat{e_1}$ is the vector with entries $\hat{e}_{1_n} = \delta_{1n}$.

The graph associated to this matrix is the one in FIG.11. The energies inside each vertex are given by subtracting the corresponding diagonal term from ω . The couplings are just the negative of the off-diagonal terms.

1. The double quantum dot

To explain the process of Gaussian elimination we will obtain the green function for the case without Majorana

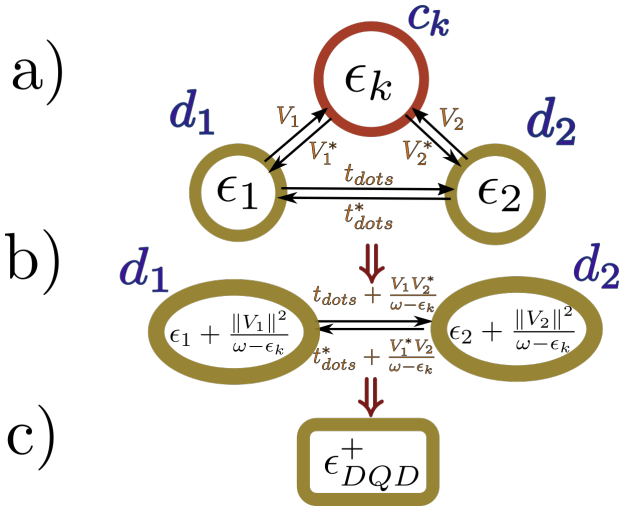

FIG. 10

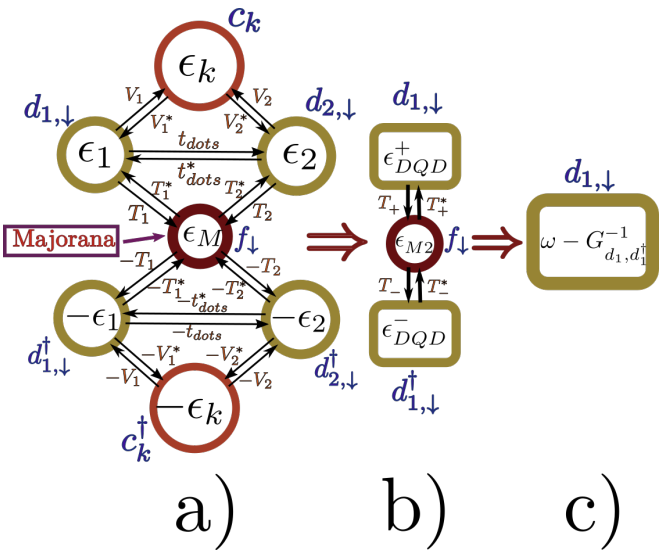

FIG. 11: Transport flow in a DQD Majorana system.

fermion ($t_1 = t_2 = 0$). The transport matrix for this system is

$$\begin{bmatrix} \omega-\epsilon_1 & -V_1 & -t_{dots} \\ -V_1^* & \omega-\epsilon_k & -V_2 \\ -t_{dots}^* & -V_2^* & \omega-\epsilon_2 \end{bmatrix}. \tag{A7}$$

The graph associated to this matrix can be observed in FIG10.a). To eliminate the vertex c_k we just need to subtract from (A7) the rank-1 matrix that cancels the row and the column corresponding to c_k. This matrix is

$$\begin{bmatrix} \frac{V_1^*V_1}{\omega-\epsilon_k} & -V_1^* & \frac{V_2V_1^*}{\omega-\epsilon_k} \\ -V_1 & \omega-\epsilon_k & -V_2 \\ \frac{V_2^*V_1}{\omega-\epsilon_k} & -V_2^* & \frac{V_2^*V_2}{\omega-\epsilon_k} \end{bmatrix}. \tag{A8}$$

The result of (A7) - (A8) is

$$\begin{bmatrix} \omega-\epsilon_1-\frac{V_1^*V_1}{\omega-\epsilon_k} & 0 & -t_{dots}-\frac{V_2V_1^*}{\omega-\epsilon_k} \\ 0 & 0 & 0 \\ -t_{dots}^*-\frac{V_2^*V_1}{\omega-\epsilon_k} & 0 & \omega-\epsilon_2-\frac{V_2V_1^*}{\omega-\epsilon_k} \end{bmatrix} \tag{A9}$$

which is depicted by the graphs in FIG.10.b). The next step is to pop-out the vertex d_2 following the same procedure. At the end, the energy inside the vertex d_1 will be

$$\epsilon^+_{DQD} = \epsilon_1 + \sum_{\mathbf{k}} \frac{V_1V_1^*}{\omega-\epsilon_{\mathbf{k}}} + \frac{\left\|t_{dots} + \sum_{\mathbf{k}} \frac{V_1V_2^*}{\omega-\epsilon_{\mathbf{k}}}\right\|^2}{\omega-\epsilon_2-\sum_{\mathbf{k}} \frac{V_2V_2^*}{\omega-\epsilon_{\mathbf{k}}}} \tag{A10}$$

and the green function of $G_{d_1 d_1^\dagger}(\omega)$ in a DQD will be given by $\frac{1}{\omega-\epsilon_{DQD}}$ (see FIG.10.c)).

2. Solution of the transport equations

The previous procedure can be generalized into the following algorithm:

1. Computing the transport equations with the second term fixed in the creation operator of the dot.
2. Setting up the graph associated to the transport system.
3. Popping out the vertexes of the graph. Each popping process carries the following steps.
   (a) Computing the extra-terms in the energies and couplings based on the walks passing through the popped vertex.
   (b) Eliminating this vertex from the graph.
   (c) Iterating till there is only one vertex.
4. The energy in the remaining vertex d is $\epsilon_d = \frac{1}{\omega - G_{d,d^\dagger}(\omega)}$.

Following these steps it is possible to solve the general case. We start with the graph in FIG.11 and we pop out the vertexes $c_k, c_k^\dagger, d_{2,\downarrow}$ and $d_{2,\downarrow}^\dagger$ in that order. The energies associated to $d_{1,\downarrow}$ and $d_{1,\downarrow}^\dagger$ will be similar to (A10) giving

$$\epsilon^\pm_{DQD} = \pm\epsilon_1 + \sum_{\mathbf{k}} \frac{V_1V_1^*}{\omega-\epsilon_{\mathbf{k}}} + \frac{\left\|\pm t_{dots} + \sum_{\mathbf{k}} \frac{V_1V_2^*}{\omega-\epsilon_{\mathbf{k}}}\right\|^2}{\omega\pm\epsilon_2-\sum_{\mathbf{k}} \frac{V_2V_2^*}{\omega-\epsilon_{\mathbf{k}}}}. \tag{A11}$$

There is also a correction in the couplings between the Majorana mode and $d_{1,\downarrow}, d_{1,\downarrow}^\dagger$ given by

$$T_\pm = \pm t_1 \pm t_2 \frac{\left(\pm t_{dots} + \sum_{\mathbf{k}} \frac{V_1V_2^*}{\omega-\epsilon_{\mathbf{k}}}\right)}{\omega\pm\epsilon_2\pm\sum_{\mathbf{k}} \frac{V_2V_2^*}{\omega-\epsilon_{\mathbf{k}}}}. \tag{A12}$$

Finally since the Majorana is in contact with dot 2, there is an extra-term appearing in the Majorana energy given by

$$\epsilon_{M2} = \omega - \epsilon_M - \frac{\frac{\omega}{\omega+\epsilon_M}\left\|t_2\right\|^2}{\omega - \epsilon_2 - \sum_{\mathbf{k}} \frac{V_2 V_2^*}{\omega - \epsilon_{\mathbf{k}}}} - \frac{\frac{\omega}{\omega+\epsilon_M}\left\|t_2\right\|^2}{\omega + \epsilon_2 - \sum_{\mathbf{k}} \frac{V_2 V_2^*}{\omega + \epsilon_{\mathbf{k}}}}. \tag{A13}$$

With all the terms of the graph in FIG.11.b) computed, it only remains to pop out vertexes $d_1^\dagger$ and $f_\downarrow$ in that order to obtain the result in equation (7).

$$G_{d_{1\downarrow}, d_{1\downarrow}^\dagger}(\omega) = \frac{1}{\omega - \epsilon_{DQD}^{+} - \frac{\left\|T_+\right\|^2}{\omega - \epsilon_{M2} - \frac{\left\|T_-\right\|^2}{\epsilon_{DQD}^{-}}}}. \tag{A14}$$